IEEE Access
Multidisciplinary | Rapid Review | Open Access Journal

Received April 30, 2022, accepted June 1, 2022, date of publication June 8, 2022, date of current version June 13, 2022.

Digital Object Identifier 10.1109/ACCESS.2022.3180739

Modifications of Limiting Current and Magnetic Insulation in a Crossed-Field Diode by a Series Resistor

ADAM M. DARR[1], (Graduate Student Member, IEEE), AND ALLEN L. GARNER[1,2,3], (Senior Member, IEEE)

[1]School of Nuclear Engineering, Purdue University, West Lafayette, IN 47906, USA
[2]Elmore Family School of Electrical and Computer Engineering, Purdue University, West Lafayette, IN 47907, USA
[3]Department of Agricultural and Biological Engineering, Purdue University, West Lafayette, IN 47907, USA

Corresponding author: Allen L. Garner (algarner@purdue.edu)

This work was supported by the Air Force Office of Scientific Research under Award FA9550-19-1-0101. The work of Adam M. Darr was also supported by Purdue Doctoral Fellowship.

ABSTRACT Adding an orthogonal magnetic field to a diode is crucial for multiple applications, including high power generation. These crossed-field diodes (CFDs) have curved electron trajectories that store current in the gap. Above a critical magnetic field referred to as the Hull cutoff, electrons emitted from the cathode fail to cross the anode-cathode gap, leading to magnetic insulation and the storage or transport of all the current. Normally, the Hull cutoff may be easily calculated from diode geometry and boundary conditions; however, dissipative effects in the circuit or the addition of a protective shunt resistor may introduce an external resistance in series that causes a mismatch between the applied voltage and the voltage drop across the gap. For non-magnetically-insulated CFDs, non-zero net current flows in the circuit due to space-charge limited current (SCLC) in the gap. In this paper, we examine several models for crossed-field SCLC below the Hull cutoff to determine the impedance of the CFD. We find that the resistor reduces the voltage drop across the gap, reducing the magnetic field necessary for magnetic insulation below the typical Hull cutoff, which in turn lowers the SCLC. One-dimensional particle-in-cell simulations show that adding the series resistor causes electron trajectories to oscillate between insulated and non-insulated states for CFDs operating within 30% of the conventional Hull cutoff; these findings are validated by further examination of the theory. Extensions to other perturbations, such as AC modulation and magnetic field tilts, are discussed.

INDEX TERMS Crossed-field, magnetic insulation, perturbations, resistor.

I. INTRODUCTION

Space-charge limited current (SCLC) represents a natural ceiling on current flow in a diode, where the electric field generated by charge carriers causes emission to become self-limiting. Child and Langmuir described the ''three-halves'' power law [1], [2] for a one-dimensional (1-D) planar gap as

$$J_{CL} = \frac{4\sqrt{2}}{9}\epsilon_0\sqrt{\frac{e}{m}}\frac{V_{gap}^{3/2}}{D^2}, \tag{1}$$

with Child-Langmuir (CL) current density J_{CL}, vacuum permittivity ϵ_0, particle charge e, particle mass m, diode gap bias voltage V_{gap}, and cathode-to-anode gap distance D.

The associate editor coordinating the review of this manuscript and approving it for publication was Norbert Herencsar.

Generalizations of this CL equation may be broadly separated into two categories: refinements in diode geometry and incorporation of additional physical phenomena. Geometric refinements include extensions of the planar 1-D CL law to various nonplanar geometries, such as coaxial cylinders [3], concentric spheres [4], two-dimensional (2-D) planar diodes [5]–[7], and bipolar flows [8]. Recently, several newly-applied theoretical tools offer frameworks that may yield analytic solutions for *any* geometry: variational calculus [9], conformal mapping [10], [11], and linking vacuum and space-charge limited electric potential in a diode [12].

Another important class of diode, often used for generating high power, is the crossed-field diode (CFD). CFDs incorporate a magnetic field B orthogonal to the electric field induced across the diode by the applied voltage. The magnitude of B causes electron trajectories to curve away from

pure cathode-to-anode motion, leading to a certain amount of stored current. Charged particles no longer reach the anode for $B > B_H$; the Hull cutoff magnetic field B_H [13] is derived from the Lorentz equation, solving for the condition when an electron just reaches the anode with zero velocity in the direction across the gap. For planar CFDs, B_H is given by [13]

$$B_H = \sqrt{\frac{2mV_{gap}}{eD^2} + \left(\frac{mu_0}{eD}\right)^2}, \tag{2}$$

with initial velocity u_0; we will assume $u_0 = 0$ in this paper. For cylindrical diodes, we may replace D in (2) with an effective gap distance, $D_{eff} \equiv 0.5R_a\left|1-\bar{a}^2\right|$, where R_a and R_c are the anode and cathode radii, respectively, and $\bar{a} \equiv R_c/R_a$ [13], [14].

For $B > B_H$, the diode is magnetically insulated such that electrons no longer reach the anode. All current is stored rather than transmitted, flowing parallel to the cathode. In real CFDs, small perturbations make this parallel flow turbulent, resulting in near-Brillouin flow, characterized by a Brillouin flow with a turbulent background [15]. Generally, laminar and turbulent SCLC predictions agree well, so most theoretical studies focus on laminar trajectories [16]. Additionally, SCLC may differ from the maximum *stable* current, often called the limiting current. These differences are negligible when $B < B_H$ [14] and do not exceed a 10% mismatch for $B > B_H$ [16], so SCLC remains an important and useful metric for CFDs.

Crossed-field SCLC, often magnetically insulated, has important implications for CFDs such as slow-wave structures [17], radar amplifiers [18], [19], Hall thrusters [20], and magnetrons [21]. A recent, comprehensive study examined Brillouin flow in magnetically insulated line oscillators (MILOs) and magnetically insulated transmission lines (MITLs), characterizing magnetic insulation via total magnetic flux [22]. Exact, analytic derivations of the limiting current in a CFD, both below and above B_H, have been available since the 1990s [23], [24]. Additional physics considered in CFDs include relativistic electron flow [25], [26], thermal effects [26]–[28], bipolar (electron-ion) interactions [29], [30], and perturbative boundary conditions [31]–[33].

This work refines SCLC for CFDs with respect to geometry and additional physical phenomena, analogous to the extensions for CL mentioned above. We build on our variational calculus approach [14], incorporating the perturbative effect of an external resistor. The injection current density J required to destabilize laminar flow into the near-Brillouin state was examined using theory and the particle-in-cell (PIC) code XPDP1 [34] for an AC modulation [31], an external resistor to represent dissipation [32], and magnetic field misalignment (tilt) [33], all for $B > B_H$. While these previous assessments focused on $B > B_H$, CFDs operating for $B < B_H$ (and, more precisely, near B_H) are also of interest [35], a regime we describe in detail.

Rather than finding the stability condition for transients, we focus on elucidating the effect of these perturbations upon SCLC, beginning with an external resistor for $B < B_H$ in this paper. Resistive crossed-field SCLC is important to understand because most field emission devices, including CFDs, use current-limiting shunt resistors to prevent damage to the device in the event of a short [36]. Adding an external series resistor to a crossed-field circuit causes initial transients, including erratic electron trajectories [23], [24]; however, the eventual SCLC condition must trend toward a steady-state due to dissipation caused by the resistor. At steady-state, magnetically insulated diodes have net zero current since all charge travels parallel to the cathode in Brillouin or near-Brillouin flow [23]. As such, we restrict our inquiry of resistive crossed-field SCLC to steady-state, non-insulated diodes ($B < B_H$). Implications of high resistances potentially causing the onset of magnetic insulation will be addressed in theory and simulation.

In this paper, we assess the critical current for a CFD with $B < B_H$ by incorporating a series resistor into three models: the critical current model that solves the Poisson equation analytically [14], [23], [24]; the anode model using non-magnetic SCLC and velocity ratios at the anode [14]; and the electric potential model, which uses the non-magnetic SCLC potential profile [14]. These models are described in detail in Section II. The critical current model matches 1-D simulations [23], [24], while the other models better describe three-dimensional experiments and simulations [14]. The impedance of all three models will be analyzed in series with a resistor by using Ohm's law. The anode and electric potential models are especially important since they may more accurately model the impedance of real CFDs. Since each of these models has been useful for different applications, each of them will be included in this work. Additionally, we will extend the anode model to cylindrical geometry.

The remainder of this paper is organized as follows. Theory will be discussed in Section II. Results, including simulation validation, will be presented in Section III. Concluding remarks will be made in Section IV.

II. THEORY

The geometry of the planar case is a grounded cathode at $x = 0$, with an anode biased to gap voltage V_{gap} at gap distance $x = D$. The geometry is infinite in $\hat{y}$ and $\hat{z}$, with an external magnetic field $\vec{B} = B\hat{z}$. The cycloidal motion of electrons emitted at the cathode is in the xy plane. The cylindrical geometry has cathode and anode at $r = R_c$ and $r = R_a$, respectively; is symmetric in $\hat{\theta}$ and infinite in $\hat{z}$; and has $\vec{B} = B\hat{z}$. Both cases consider electrons emitted from the cathode with zero initial velocity ($u_0 = 0$). An external resistor R and voltage source with strength V_{app} in series with the diode will be analyzed.

The critical current model, denoted by subscript c throughout, was initially derived for $B < B_H$ from a transit time argument to find the limiting current [23] and later using variational calculus to find the SCLC condition [14]. Both approaches reached the same solution [14]; note, limiting current and SCLC results may differ slightly for magnetically

insulated ($B > B_H$) CFDs [16], [37]. This model solves the Poisson and Lorentz equations from first principles to maximize current density in the gap. For zero initial velocity $u_0 = 0$ used throughout this paper, the SCLC condition is zero electric field at the cathode [2]. For $B < B_H$, the critical current density J_c can be expressed analytically by (cf. (13)-(15) of [23])

$$\frac{J_c}{J_{CL}} = \frac{9}{4}\frac{y^2}{\left(1+y^2\right)^{3/2}\left[h\left(y\right)\right]^2}, \tag{3}$$

with J_{CL} given by (1) and $h\left(y\right)$ and y described by

$$y = \begin{cases} \dfrac{1}{h^2}\left[\sin^{-1}\left(h\right) - h\sqrt{1-h^2}\right], & 0 < y < \dfrac{\pi}{2} \\ \dfrac{1}{h^2}\left[\dfrac{\pi}{2} + \cos^{-1}\left(h\right) + h\sqrt{1-h^2}\right], & y > \dfrac{\pi}{2} \end{cases} \tag{4}$$

and

$$y = \frac{\left(B/B_H\right)}{\sqrt{1-\left(B/B_H\right)^2}}, \tag{5}$$

respectively.

The anode model, denoted by subscript a, assumes the total current density, including stored current in Brillouin-type flow, cannot exceed J_{CL}. This is a reasonable assumption, since for $0 < B < B_H$, $J_c < J_{CL}$ [23]. The current density in $\hat{x}$ is constant due to steady-state continuity $\vec{J} = \rho\vec{v}$, so the highest total current density is at the anode. The emission current density J_a is given by (cf. (22) of [14])

$$\frac{J_a}{J_{CL}} = \sqrt{1-\left(B/B_H\right)^2}. \tag{6}$$

The electric potential model, denoted by subscript e, calculates average current density using cathode-to-anode velocity from the Lorentz equation and assuming the electric potential profile is identical to the $B = 0$ case [1, 2]. The emission current density J_e for this model is given by (cf. (24) of [14])

$$\frac{J_e}{J_{CL}} = \frac{2}{3}\frac{\left(B/B_H\right)^3}{\sin^{-1}\left(B/B_H\right) - \left(B/B_H\right)\sqrt{1-\left(B/B_H\right)^2}}. \tag{7}$$

Equations (3)-(7) may be multiplied by an arbitrary emission area S to find the total current $I = JS$. We may then calculate the impedance of the diode gap, $Z_{gap} = V_{gap}/I$. Ohm's law with an external resistor in series is

$$V_{app} = V_{gap} + RI = \left(Z_{gap} + R\right)JS. \tag{8}$$

As a consequence of (8), B_H from (2) cannot be calculated simply with $V_{gap} = V_{app}$. Instead, adding the resistor perturbs B_H. We calculate this perturbed Hull cutoff $\tilde{B}_H$ by substituting V_{gap} from (8) into (2). Equations (3)-(7) must be evaluated using $\tilde{B}_H$ in place of B_H to reflect the final steady-state. This complicates our analysis, since J, $\tilde{B}_H$, and V_{gap} must be solved simultaneously, with Z_{gap} varying depending upon the model used.

We can write the gap impedance Z_c associated with J_c as

$$Z_c = Z_0\frac{4}{9}\frac{\left(1+y^2\right)^{3/2}\left[h\left(y\right)\right]^2}{y^2}, \tag{9}$$

with

$$Z_0 \equiv \frac{9mD}{4eS\epsilon_0\tilde{B}_H}. \tag{10}$$

For $B = 0$, Z_0 is the nominal impedance corresponding to the non-magnetic CL equation (1), solved from Ohm's law (8). Note, Z_c cannot be found analytically because (3) includes the inverse function $h\left(y\right)$, which must be obtained by simultaneously solving (4) and (5). Also, Z_0 varies with R, due to $\tilde{B}_H$ dependence.

Equations (6) and (7) readily admit exact solutions for the gap impedances Z_a and Z_e, as

$$Z_a = Z_0\frac{1}{\sqrt{1-\left(B/\tilde{B}_H\right)^2}} \tag{11}$$

and

$$Z_e = Z_0\frac{3}{2\left(B/\tilde{B}_H\right)^3} \times\left[\sin^{-1}\left(B/\tilde{B}_H\right) - \left(B/\tilde{B}_H\right)\sqrt{1-\left(B/\tilde{B}_H\right)^2}\right], \tag{12}$$

respectively.

The impedance relations (9)-(12) depend upon S, D, B, and R, which nonlinearly contribute to changes in $\tilde{B}_H$ and V_{gap}. As an important consequence, a device with constant B and V_{app} may still tune gap impedance using a variable resistor, which reduces V_{gap} according to

$$V_{gap} = \frac{V_{app}}{1 + R/Z_{gap}}, \tag{13}$$

where Z_{gap} is given by any of (9)-(12). It is also illustrative to recast (13) using the Hull cutoff definition from (1), yielding

$$\tilde{B}_H^2 = \frac{B_H^2}{1 + R/Z_{gap}}. \tag{14}$$

To supplement these planar models, we may derive an analogous anode model for cylindrical diode impedance. In cylindrical coordinates, SCLC at the cathode for $B = 0$, J_{SCLC}, is given by [9]

$$J_{SCLC} = \frac{4\sqrt{2}}{9}\epsilon_0\sqrt{\frac{e}{m}}\frac{V^{3/2}}{R_c^2\left(\left|\ln\bar{a}\right|\right)^2}, \tag{15}$$

where $\bar{a} \equiv R_c/R_a$ arises from the curvature of the electrodes. Continuity means the ratio of current densities at the cathode and anode is $1/\bar{a}$, since total current is constant [14]. Because this is an anode model, we assume the total current at the anode cannot exceed emitted current, or $\left|\vec{J}\right| = J_{SCLC}/\bar{a}$, once cathode emission current density reaches the anode. Using

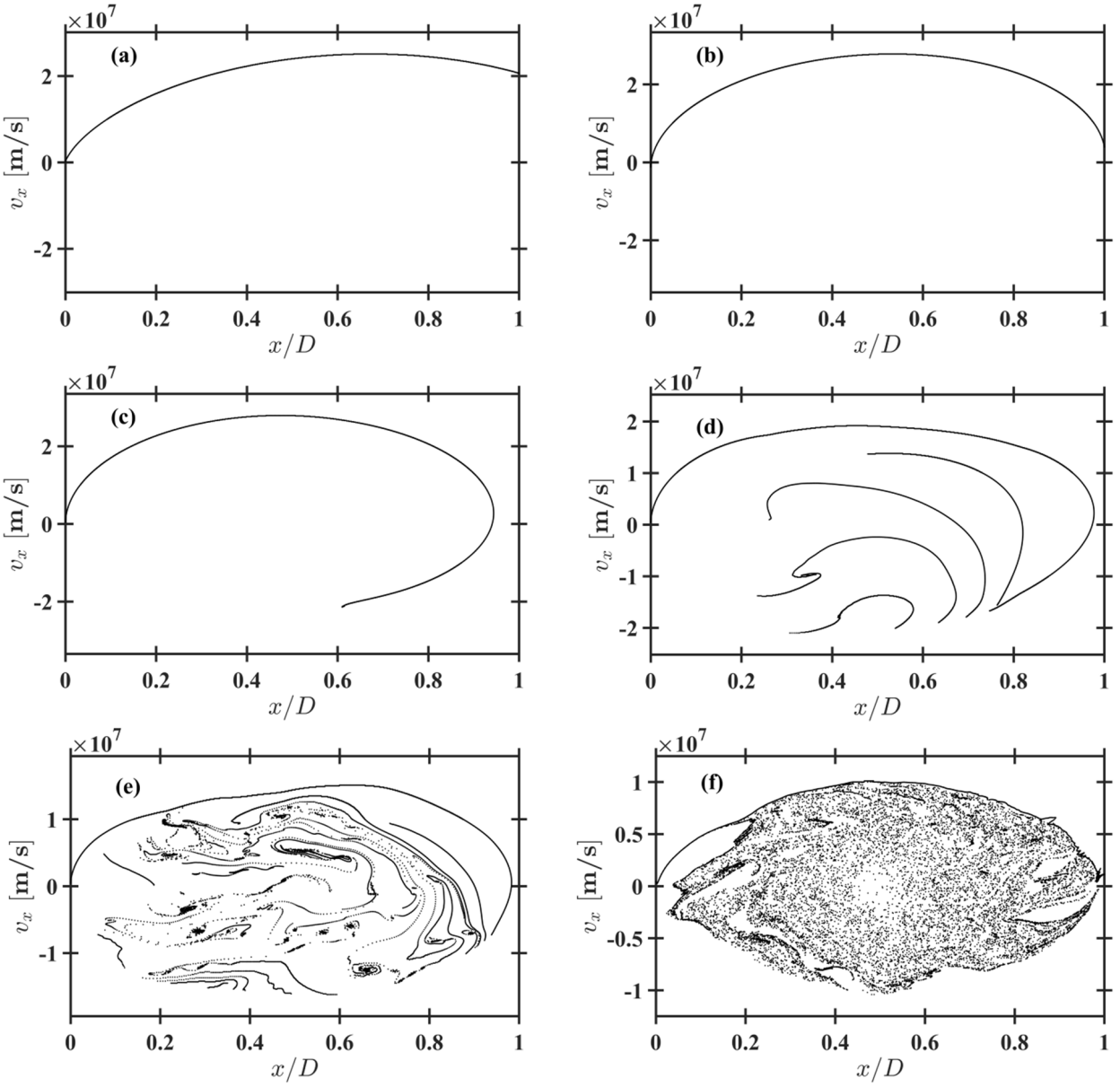

FIGURE 1. Snapshots of $\hat{x}$ velocity v_x as a function of normalized position x/D, where D is the gap distance (2.16 mm), for electrons in XPDP1 [34] for (a) $R = 0\ \Omega$ and (b) $R = 4\ \Omega$, both stable steady-states and (c)-(f) $R = 7\ \Omega$. Applied voltage 12 kV, emission area 14.92 cm^2, magnetic field 0.1625 T (95% of Hull cutoff, $B_H = 0.171$ T). Panels (a) and (b) are stable steady-states; the other snapshots are at specific times: (c) 0.194 ns (d) 1.342 ns, (e) 3.822 ns, and (f) 47.35 ns.

continuity $\vec{J} = \rho\vec{v}$, we note $\rho = v_\theta/J_\theta = v_r/J_r$, where J_θ is stored current. From (6) and (7b) of [14], $v_\theta^2/v_r^2 = \left(B_H/B\right)^2 - 1$. We define the cylindrical anode model current density $J_{a,cyl}$ as $J_{a,cyl} \equiv J_r$. Converting from anode to cathode by multiplying $J_{a,cyl}$ by $\bar{a}$ yields

$$\frac{J_{a,cyl}}{J_{SCLC}} = \sqrt{1 - (B/B_H)^2}. \tag{16}$$

Note that while (16) appears superficially identical to the planar analogue (6), B_H is defined by the effective gap distance noted earlier ($D_{eff} \equiv 0.5R_a\left|1 - \bar{a}^2\right|$) and $J_{SCLC} \neq J_{CL}$ for cylindrical geometries [9], [10]. The corresponding gap impedance $Z_{a,cyl}$ can be solved using (13) in (8), giving

$$Z_{a,cyl} = Z_{0,cyl}\frac{1}{\sqrt{1 - \left(B/\tilde{B}_H\right)^2}}, \tag{17}$$

with

$$Z_{0,cyl} = \frac{9m\left(R_c\left|\ln\bar{a}\right|\right)^2}{4eS\epsilon_0\tilde{B}_H D_{eff}}. \tag{18}$$

Just as with planar Z_0 from (10), for $B = 0$, $Z_{0,cyl}$ is the nominal impedance of a cylindrical SCLC device, as derived from (8) and (12).

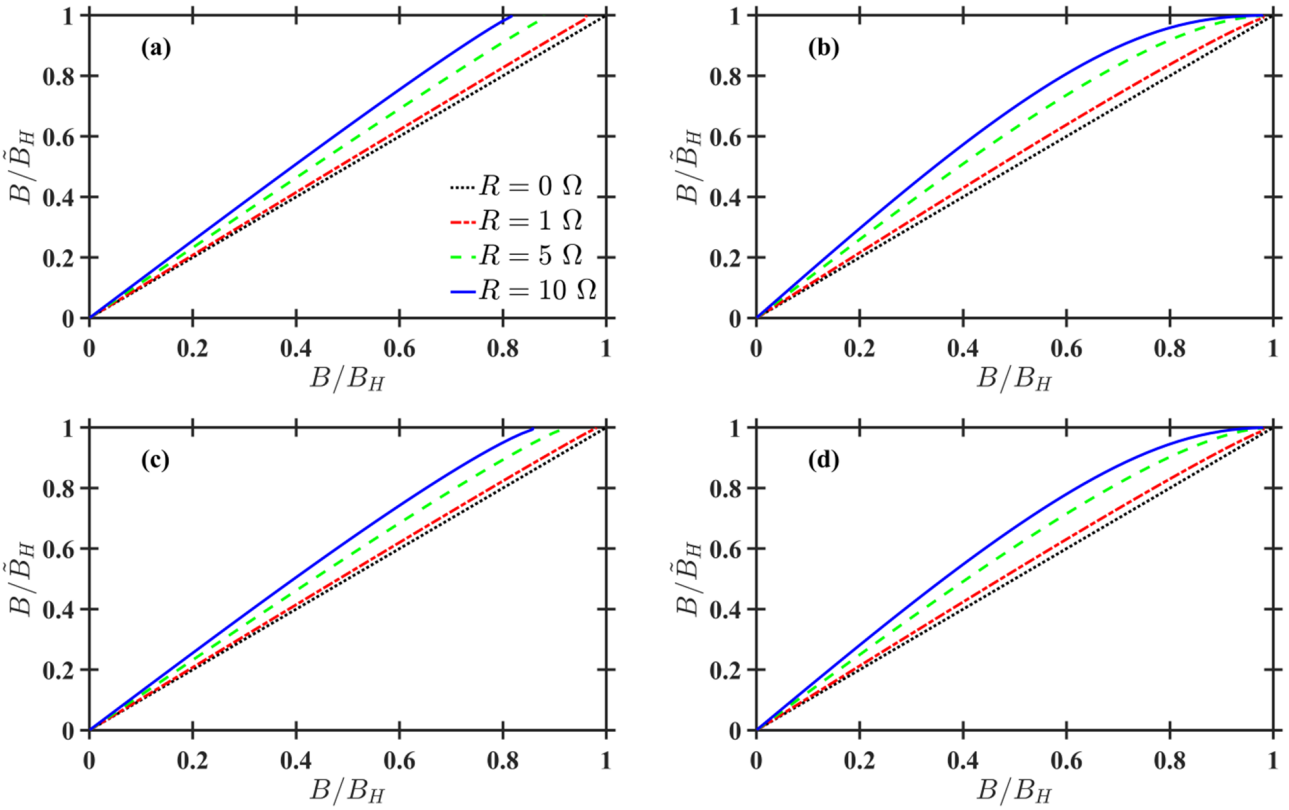

FIGURE 2. Ratio of magnetic field B to the perturbed Hull cutoff $\tilde{B}_H$ as a function of the ratio of B to the initial Hull cutoff B_H for several resistances R for the (a) critical current model, (b) anode model, (c) electric potential model, (d) anode model for cylinders (cathode radius 2.16 mm, anode radius 4.32 mm). Constant diode properties are applied voltage 12 kV, emission area 14.92 cm^2, and gap distance 2.16 mm.

Note that we considered deriving a cylindrical version of the electric potential model [14] using $\phi(r)$ from [9], but the integral could not be evaluated analytically or numerically.

III. RESULTS

Given the impedance relations derived above (9)-(12), (17), and (18), and Ohm's law, we may analyze CFDs with resistance in series in the steady-state. Note that while a transient model is available above the Hull cutoff ($B > B_H$) [16], all the net current is parallel to the cathode in steady-state. From Ohm's law, the resistor will not influence the final steady-state when real current $I = 0$, since no voltage is dissipated r the resistor ($V\_R = 0$).

This raises an important question: how might a non-insulated ($B < B_H$ when $R = 0$) diode act when placed in series with a resistor large enough to reduce perturbed $\tilde{B}_H$ such that $B > \tilde{B}_H$? We motivate this discussion with a thought experiment. Suppose a planar diode operates with $B/B_H = 0.95$, just below the Hull cutoff. Regardless of the model used, the diode completes the circuit with some finite initial current density J_i for any resistance that predicts final $B/\tilde{B}_H < 1$. Figure 1(b) shows the final steady-state of a CFD perturbed with a 4 Ω resistor that still results in stable flow in XPDP1 [34] simulations, matching theoretical assumptions and resembling the $R = 0$ case in Fig. 1(a). The steady-state trajectory has a much lower energy than the $R = 0$ case in Fig. 1(a) and has a space-charge limit only 36.5% of the unperturbed system. Moreover, the electron velocity in the x-direction decreases noticeably with increasing resistance. Further increasing the resistance eventually makes the electrons undergo velocity in the negative x-direction before reaching the anode, resulting in the Brilluoin state. This is analogous to the misaligned CFD studied previously [33]. Introducing a magnetic field component in the x-direction eliminated magnetic insulation, causing the electrons to traverse the gap. Increasing the tilt or the applied current density changed the number of "loops" that the electrons made as they crossed the gap, resulting in bands of stability at the number of loops changed due to the buildup of space-charge at the turning points. The decrease in velocity in the x-direction with increasing resistance is analogous in that it increases the space-charge in the gap that induces the instability.

Assuming fixed B, V_{app}, and D, (2) gives $B/\tilde{B}_H \propto V_{gap}^{-1/2}$ in the final state, so any decrease in the gap voltage V_{gap} will increase $B/\tilde{B}_H$. Introducing a series resistance suddenly (e.g., opening a switch) will instantaneously decrease V_{gap}, but will not decrease the total current immediately. Even as SCLC emission characteristics change, the total amount of charge flowing in the gap (and, correspondingly, current density) decreases only as charge is collected at the anode or cathode. By Ohm's law, some of the applied voltage V_{app} will be applied across the resistor as $V_R = IR = (J_i A)\,R$, where J_i is the injected current density, rather than across the gap. A sufficiently high R such that $V_R \approx 0.2\ V_{app}$ would

instantaneously yield $B/\tilde{B}_H > 1.05$, indicating magnetic insulation in the steady-state. Since magnetically insulated diodes have no real current, as the system attempts to relax to a steady-state I and V_R will decrease while V_{gap} increases. Since $I = 0$ for any $B > \tilde{B}_H$, the real current will ultimately decrease enough to restore $B/\tilde{B}_H < 1$. In turn, I will once again increase until $B/\tilde{B}_H > 1$. We hypothesize an onset of magnetic insulation due to the reduction of V_{gap}, followed by periodic insulated and non-insulated behaviors. Since the resistor is a dissipative element, the magnitude of these bimodal oscillations will most likely damp until a quasi-steady-state is reached with $B \approx \tilde{B}_H$.

To assess the possibility of onset of magnetic insulation from resistive effects, we performed planar simulations in XPDP1, a 1d3v (one-dimensional in space, three-dimensional in velocity) particle-in-cell (PIC) simulation code [34]. The simulations used $V_{app} = 12,000$ V and $D = 2.16$ mm, giving $B_H = 0.171$T [24]. Fig. 1 shows the velocity in $\hat{x}$, v_x, as a function of normalized position x/D at several time steps for $B/B_H = 0.95$. Figs. 1(a) and 1(b) show the stable steady-states for $R = 0\ \Omega$ and $R = 4\ \Omega$, respectively, while Figs. 1(c)-(f) show the time-progression for $R = 7\ \Omega$. For reference, with $R = 0$, $Z_0 = 12.24\ \Omega$ for this magnetic field. Fig. 1(c) shows the first cycloid missing the anode, demonstrating the onset of magnetic insulation. However, not all of the first cycloid misses the anode; subsequent cessation of magnetic insulation truncates the insulated part of the cycloid, which continues to oscillate between the cathode and anode. This pattern of alternating magnetic insulation and non-insulation fills the gap with insulated cycloid elements oscillating and deforming, as shown in Fig. 1(d). This bimodal pattern continues for many dozens of oscillations, with magnetically insulated segments becoming less frequent and smaller as space-charge from prior, insulated segments builds in the center. Fig. 1(e) shows a collapse of the central charge into a turbulent state surrounded by an imperfect ring reminiscent of the first partial cycloid in Fig. 1(b). The final state of this diode is shown in Fig. 1(f), where bimodality has collapsed into a high velocity sheath in $v_x - x$ space surrounding a turbulent, lower velocity core. The number of particles eventually saturates since XPDP1 injects electrons directly, and the behavior oscillates about a single steady-state with characteristics of both insulated and non-insulated current flow, or $B \approx \tilde{B}_H$. Future work may specifically account for the emission mechanisms by using a field or thermionic (or combined thermo-field) emission model to avoid the issues caused by direct injection.

Physically, some elements of particular cycloids are magnetically insulated when V_R is highest and V_{gap} is lowest. This means those insulated elements gain less energy; indeed, they have insufficient energy to cross the gap or return to the cathode once V_{gap} later increases. This trapped charge permanently increases the amount of space-charge within the gap, although some of the trapped charge may eventually migrate to the anode upon reaching the quasi-steady-state.

The onset of magnetic insulation and bimodal behavior may be predicted by examining the perturbation of B/B_H to $B/\tilde{B}_H$ for the various impedance models. Fig. 2 shows the change from the initial ratio B/B_H to the perturbed ratio $B/\tilde{B}_H$ for several constant values of R, compared to the $R = 0$ baseline $B_H = \tilde{B}_H$. In effect, higher $B/\tilde{B}_H$ is caused by a reduction in V_{gap} and $\tilde{B}_H$. The onset of magnetic insulation, and subsequent bimodal oscillations, is indicated whenever $B/\tilde{B}_H$ exceeds unity. This behavior, seen in simulations, does not occur for the anode models in Figs. 2(b) and 2(d), which instead only predict $B/\tilde{B}_H$ *asymptotically approaching* unity. For an alternative perspective, Fig. 3 shows the effect of a variable resistor on a gap. This more clearly shows how increased resistance either brings $B/\tilde{B}_H$ directly to unity (onset of magnetic insulation), or instead only approaches unity for the anode models.

The anode models fail to predict the onset of magnetic insulation we observe in simulations. Unlike the other models, the current densities predicted by the anode models in (11) and (16) approach zero as $B/B_H \to 1^-$. Thus, current vanishes at the limit of magnetic insulation, so V_R becomes negligible near the Hull cutoff in the anode models. The planar anode model is the best fit to experimental data [14], so these results may indicate that real CFDs will not experience onset of magnetic insulation or bimodal electron flow states. Even without onset of magnetic insulation, the anode model still demonstrates how R may tune $\tilde{B}_H$, and thus device behavior. Other small dissipative elements in the circuit can contribute to an effective R higher than the nominal shunt resistance, which could result in significantly lower currents than expected. Simulations with more than one physical dimension or experiments may be needed to more fully understand this phenomenon, as previously suggested [14]. The prevalence of the critical current model [23], [24] make these one-dimensional results a relevant step forward in understanding the complete picture of CFD behavior.

Though the anode models do not predict onset of magnetic insulation, we can examine the critical current and electric potential models by taking limits as $B/\tilde{B}_H \to 1^-$. For the critical current model, $J_c \to (9J_{CL})/(4\pi)$ [23]; the electric potential model limit can be found by direct substitution as $J_e \to (4J_{CL})/(3\pi)$. These can be used directly to calculate $Z_{gap} = V_{gap}/(JS)$ in (14), where we also divide both sides by B^2 to obtain

$$\frac{\tilde{B}_H^2}{B^2} = \frac{B_H^2/B^2}{1 + RJS/V_{gap}}. \tag{19}$$

Noting that $B/\tilde{B}_H = 1$ for onset of magnetic insulation, solving (19) for R yields

$$R = \frac{V_{gap}}{JS}\left[\left(\frac{B}{B_H}\right)^{-2} - 1\right]. \tag{20}$$

Using appropriate limits and substitutions, critical resistances for onset of magnetic insulation for the critical current

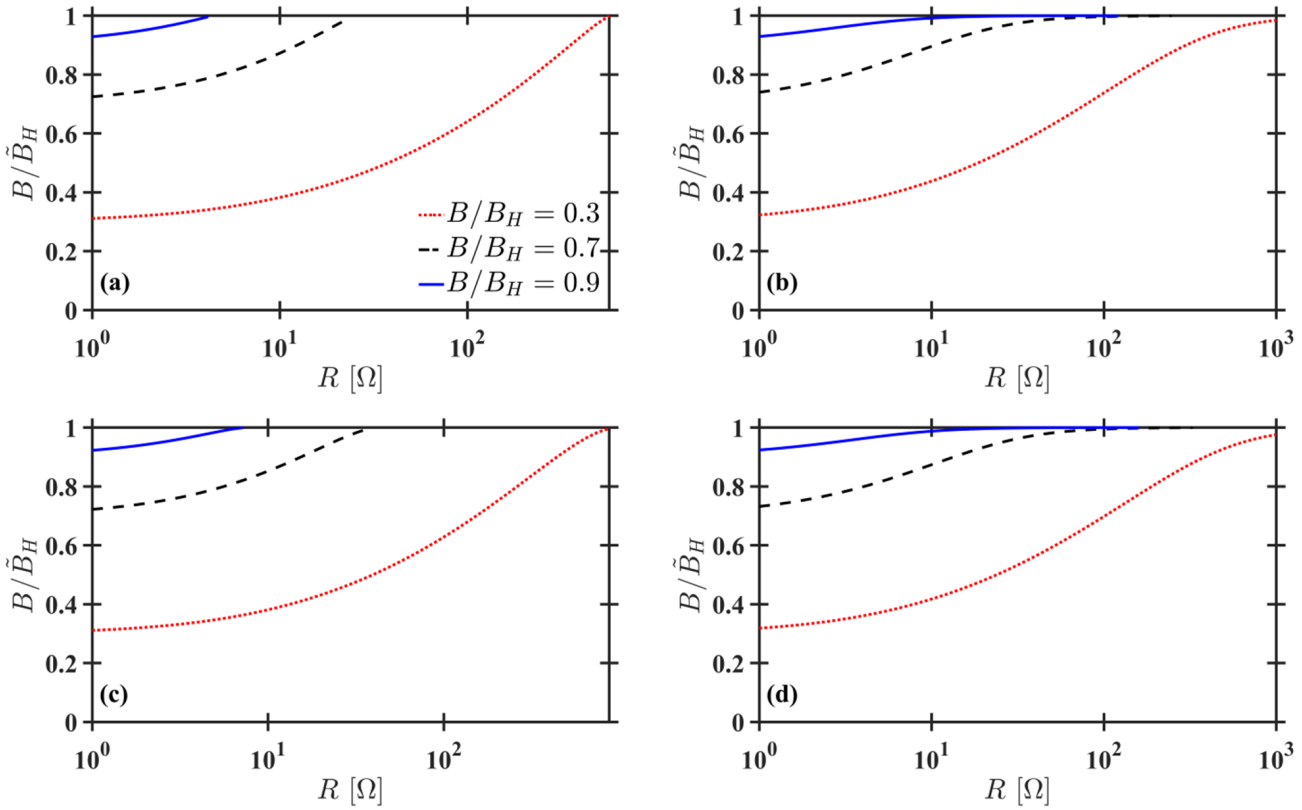

FIGURE 3. Ratio of magnetic field B to the perturbed Hull cutoff $\tilde{B}_H$ as a function of external resistance R for constant ratio of B to the initial Hull cutoff B_H for the (a) critical current model, (b) anode model, (c) electric potential model, (d) anode model for cylinders (cathode radius 2.16 mm, anode radius 4.32 mm). Constant diode properties are applied voltage 12 kV, emission area 14.92 cm^2, and gap distance 2.16 mm.

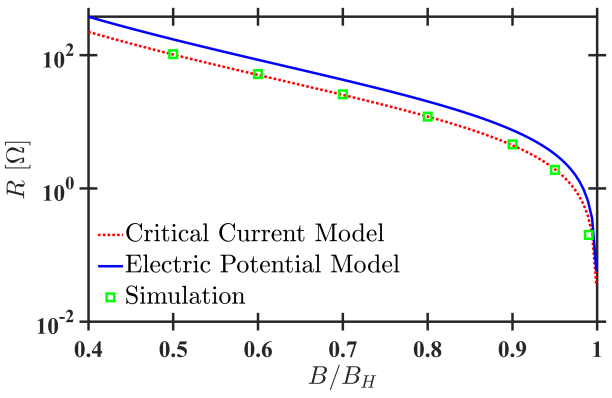

FIGURE 4. Critical resistance R leading to onset of magnetic insulation as a function of the ratio of B to the non-perturbed Hull cutoff B_H using the critical current model and electric potential models according to (21), and from simulations using XPDP1 [34]. Constant diode properties are applied voltage 12 kV, emission area 14.92 cm^2, and gap distance 2.16 mm.

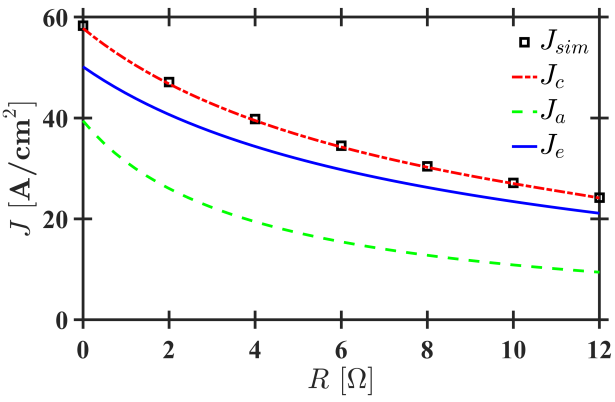

FIGURE 5. Current density J as a function of resistance R from XPDP1 [34] simulations J_{sim}, the critical current model J_c, the anode model J_a, and the electric potential model J_e. Constant diode properties are applied voltage 12 kV, emission area 14.92 cm^2, and gap distance 2.16 mm.

model R_c and electric potential model R_e are

$$R_c = \frac{\pi m D}{eB\epsilon_0 S}\left[\left(\frac{B}{B_H}\right)^{-2} - 1\right];$$
$$R_e = \frac{27\pi m D}{16eB\epsilon_0 S}\left[\left(\frac{B}{B_H}\right)^{-2} - 1\right]. \quad (21)$$

Fig. 4 plots (21) along with XPDP1 simulations. In simulation, we look for two characteristics: minimum R to induce onset of magnetic insulation and minimum J to meet the SCLC condition of zero electric field at the cathode. We define critical R when both these conditions are satisfied simultaneously. As expected, the critical current model agrees well with simulations, though we must again caution that neither represents experimental data appropriately [14].

Finally, Fig. 5 shows the consequences of an external resistor on J. The planar models are compared to planar XPDP1 simulations, with J_{sim} found from the SCLC condition as

described earlier. The cylindrical anode model has the same trend as the planar anode model, but with different B_H and J_{SCLC} normalizations, and as such is omitted. As expected, the simulation results again agree well with the critical current model. For the critical current model, onset of magnetic insulation occurs for $R \approx 12\ \Omega$, which we use as the right-hand termination of the abscissa. The critical current, anode, and electric potential models show reductions in J of 58.2%, 76.1%, and 57.9%, respectively, from 0 to 12 Ω. The largest slope in terms of current density loss occurs at low R, so even small resistances may significantly lower expected output of a CFD.

IV. CONCLUSION

By applying Ohm's law to several models of crossed-field current density, we have shown how an external resistance R in series can significantly alter diode behavior. This resistance could represent various factors, from dissipation inherent in the system to shunt resistors. The Hull cutoff field B_H is perturbed to a lower value $\tilde{B}_H$ due to changes in the gap voltage V_{gap}, causing the diode to trend closer to magnetic insulation $B/B_H = 1$. This reduces the emitted current density, since crossed-field SCLC is lower for larger ratios of $B/\tilde{B}_H$ and smaller V_{gap}. This has important implications for both designed resistances, which can tune the final, perturbed $\tilde{B}_H$, and for unintended resistances (i.e., dissipation), which lower limiting current in the diode. We showed that adding a 12 Ω resistor to realistic crossed-field diode (CFD) geometries can reduce the limiting current by over 50%. Future work may investigate the effects of an initial velocity [23], [24], [38]–[40], including non-uniform distributions like Maxwell-Boltzmann [41], which generally increase the space-charge limit and may possibly mitigate the reduction in limiting current.

For ratios of B/B_H already close to unity, XPDP1 [34] simulations showed that electron flow oscillated between magnetically insulated and non-insulated states with this bimodal behavior eventually settling into a steady-state with characteristics of insulated and non-insulated flows. Future analysis may incorporate AC modulation, including combined transients with the resistor as shown in Fig. 1. These simulations had constant injected current, so future studies with direct field or thermionic emission may display a different final steady-state, or even permanent bimodal behavior. It will also be important to model finite-dimensional (2D, 3D) diodes in future studies, especially for nonuniform SCLC [42]. The techniques of conformal mapping [10] and vacuum capacitance analysis [12] have already been used for non-magnetic pin-to-plate geometries [11]. We have already characterized electron emission in regimes where multiple mechanisms may contribute for non-magnetic diodes [43]–[45] and are currently carrying out similar investigations for CFDs [46]. We also used several crossed-field SCLC models to predict the onset of magnetic insulation. We note that the anode models, which most successfully predict experimental data [14], do not predict onset of magnetic insulation, further motivating future work with fully three-dimensional simulations and new experiments to investigate this phenomenon.

REFERENCES

[1] C. D. Child, "Discharge from hot CaO," *Phys. Rev.*, vol. 32, pp. 492–511, May 1911.

[2] I. Langmuir, "The effect of space charge and residual gases on thermionic currents in high vacuum," *Phys. Rev.*, vol. 2, no. 6, pp. 450–486, Dec. 1913.

[3] I. Langmuir and K. B. Blodgett, "Currents limited by space charge between coaxial cylinders," *Phys. Rev.*, vol. 22, no. 4, pp. 347–356, Oct. 1923.

[4] I. Langmuir and K. B. Blodgett, "Currents limited by space charge between concentric spheres," *Phys. Rev.*, vol. 24, no. 1, pp. 49–59, Jul. 1924.

[5] J. W. Luginsland, Y. Y. Lau, and R. M. Gilgenbach, "Two-dimensional Child–Langmuir law," *Phys. Rev. Lett.*, vol. 77, no. 22, pp. 4668–4670, 1996.

[6] Y. Y. Lau, "Simple theory for the two-dimensional Child–Langmuir law," *Phys. Rev. Lett.*, vol. 87, no. 27, Dec. 2001, Art. no. 278301.

[7] B. Ragan-Kelley, J. Verboncoeur, and Y. Feng, "Two-dimensional axisymmetric Child–Langmuir scaling law," *Phys. Plasmas*, vol. 16, no. 10, 2009, Art. no. 103102.

[8] M. Y. Liao, R. H. Yao, and Y. B. Zhu, "Space charge limited current for bipolar flow with uniform initial velocity," *Phys. Plasmas*, vol. 28, no. 6, Jun. 2021, Art. no. 063508.

[9] A. M. Darr and A. L. Garner, "A coordinate system invariant formulation for space-charge limited current in vacuum," *Appl. Phys. Lett.*, vol. 115, no. 5, Jul. 2019, Art. no. 054101.

[10] N. R. S. Harsha and A. L. Garner, "Applying conformal mapping to derive analytical solutions of space-charge-limited current density for various geometries," *IEEE Trans. Electron Devices*, vol. 68, no. 1, pp. 264–270, Jan. 2021.

[11] N. R. S. Harsha and A. L. Garner, "Analytic solutions for space-charge-limited current density from a sharp tip," *IEEE Trans. Electron Devices*, vol. 68, no. 12, pp. 6525–6531, Dec. 2021.

[12] N. R. S. Harsha, M. Pearlman, J. Browning, and A. L. Garner, "A multi-dimensional Child–Langmuir law for any diode geometry," *Phys. Plasmas*, vol. 28, no. 12, Dec. 2021, Art. no. 122103.

[13] A. W. Hull, "The effect of a uniform magnetic field on the motion of electrons between coaxial cylinders," *Phys. Rev.*, vol. 18, no. 1, pp. 31–57, 1921.

[14] A. M. Darr, R. Bhattacharya, J. Browning, and A. L. Garner, "Space-charge limited current in planar and cylindrical crossed-field diodes using variational calculus," *Phys. Plasmas*, vol. 28, no. 8, Aug. 2021, Art. no. 082110.

[15] D. H. Simon, Y. Y. Lau, G. Greening, P. Wong, B. W. Hoff, and R. M. Gilgenbach, "Stability of Brillouin flow in planar, conventional, and inverted magnetrons," *Phys. Plasmas*, vol. 22, no. 8, Aug. 2015, Art. no. 082104.

[16] P. J. Christenson, "Equilibrium, stability, and turbulence in cycloidal electron flows in crossed electric and magnetic fields," Ph.D. dissertation, Dept. Nucl. Eng., Univ. Michigan, Ann Arbor, MI, USA, 1996.

[17] D. H. Simon, Y. Y. Lau, G. Greening, P. Wong, B. Hoff, and R. M. Gilgenbach, "Stability of Brillouin flow in the presence of slow-wave structures," *Phys. Plasmas*, vol. 23, Sep. 2016, Art. no. 092101.

[18] S. C. Exelby, G. B. Greening, N. M. Jordan, D. A. Packard, D. Simon, Y. Y. Lau, B. W. Hoff, and R. M. Gilgenbach, "High-power recirculating planar crossed-field amplifier design and development," *IEEE Trans. Electron Devices*, vol. 65, no. 6, pp. 2361–2365, Jun. 2018.

[19] S. C. Exelby, Jr., "Recirculating planar crossed-field amplifiers," Ph.D. dissertation, Dept. Nucl. Eng. Radiolog. Sci., Univ. Michigan, Ann Arbor, MI, USA, 2019.

[20] J. P. Boeuf and L. Garrigues, "E × B electron drift instability in Hall thrusters: Particle-in-cell simulations vs. theory," *Phys. Plasmas*, vol. 25, no. 6, Jun. 2018, Art. no. 061204.

[21] D. Andreev, A. Kuskov, and E. Schamiloglu, "Review of the relativistic magnetron," *Matter Radiat. Extremes*, vol. 4, no. 6, Nov. 2019, Art. no. 067201.

[22] Y. Y. Lau, D. A. Packard, C. J. Swenson, J. W. Luginsland, D. Li, A. Jassem, N. M. Jordan, R. D. McBride, and R. M. Gilgenbach, "Explicit Brillouin flow solutions in magnetrons, magnetically insulated line oscillators, and radial magnetically insulated transmission lines," *IEEE Trans. Plasma Sci.*, vol. 49, no. 11, pp. 3418–3437, Nov. 2021.

[23] Y. Y. Lau, P. Christenson, and D. Chernin, "Limiting current in a crossed-field gap," *Phys. Plasmas*, vol. 5, no. 12, pp. 4486–4489, 1993.

[24] P. Christenson and Y. Y. Lau, "Transition to turbulence in a crossed-field gap," *Phys. Plasmas*, vol. 1, no. 12, pp. 3725–3727, 1994.
[25] M. Lopez, Y. Y. Lau, J. W. Luginsland, D. W. Jordan, and R. M. Gilgenbach, "Limiting current in a relativistic diode under the condition of magnetic insulation," *Phys. Plasmas*, vol. 10, no. 11, pp. 4489–4493, Nov. 2003.
[26] S. Marini, F. B. Rizzato, and R. Pakter, "Space-charge and thermal effects in relativistic crossed-field devices," *Phys. Plasmas*, vol. 25, no. 6, Jun. 2018, Art. no. 063111.
[27] S. Marini, F. B. Rizzato, and R. Pakter, "Thermal effects and space-charge limited transition in crossed-field devices," *Phys. Plasmas*, vol. 21, no. 8, Aug. 2014, Art. no. 083111.
[28] D. Chernin, A. Jassem, and Y. Y. Lau, "Thermal electron flow in a planar crossed-field diode," *IEEE Trans. Plasma Sci.*, vol. 48, no. 9, pp. 3109–3114, Sep. 2020.
[29] B. S. Stutzman and J. W. Luginsland, "Loss of magnetic insulation in a crossed-field diode: Ion and collisional effects," *IEEE Trans. Plasma Sci.*, vol. 38, no. 8, pp. 2010–2015, Aug. 2010.
[30] M. Y. Liao, R. H. Yao, and Y. B. Zhu, "Space charge limited current for bipolar flow in a crossed-field vacuum gap," *Vacuum*, vol. 196, Feb. 2022, Art. no. 110744.
[31] P. J. Christenson and Y. Y. Lau, "One-dimensional modulational instability in a crossed-field gap," *Phys. Rev. Lett.*, vol. 76, no. 18, pp. 3324–3327, 1996.
[32] P. J. Christenson, D. P. Chernin, A. L. Garner, and Y. Y. Lau, "Resistive destabilization of cycloidal electron flow and universality of (near-) Brillouin flow in a crossed-field gap," *Phys. Plasmas*, vol. 3, no. 12, pp. 4455–4462, Dec. 1996.
[33] A. L. Garner, Y. Y. Lau, and D. Chernin, "Collapse of cycloidal electron flows induced by misalignments in a magnetically insulated diode," *Phys. Plasmas*, vol. 5, pp. 2447–2452, Jun. 1998.
[34] J. P. Verboncoeur, M. V. Alves, V. Vahedi, and C. K. Birdsall, "Simultaneous potential and circuit solution for 1D bounded plasma particle simulation codes," *Comput. Phys.*, vol. 104, no. 2, pp. 321–328, 1993.
[35] D. A. Packard, Y. Y. Lau, E. N. Guerin, C. J. Swenson, S. V. Langellotti, A. Jassem, D. Li, N. M. Jordan, J. W. Luginsland, R. D. McBride, and R. M. Gilgenbach, "Theory, simulation, and experiments on a magnetically insulated line oscillator (MILO) at 10 kA, 240 kV near hull cutoff condition," *Phys. Plasmas*, vol. 28, no. 12, Dec. 2021, Art. no. 123102.
[36] R. Gałek and P. Strzelczyk, "Velocity profiles of an electrohydrodynamic flow generator: CFD and experiment," *J. Electrostatics*, vol. 99, pp. 19–30, May 2019.
[37] P. J. Christenson and Y. Y. Lau, "Erratum: 'Transition to turbulence in a crossed-field gap' [Phys. Plasmas 1, 3725 (1994)]," *Phys. Plasmas*, vol. 3, p. 4293, Nov. 1996.
[38] G. Jaffé, "On the currents carried by electrons of uniform initial velocity," *Phys. Rev.*, vol. 65, nos. 3–4, pp. 91–98, Feb. 1944.
[39] P. V. Akimov, H. Schamel, H. Kolinsky, A. Y. Ender, and V. I. Kuznetsov, "The true nature of space-charge-limited currents in electron vacuum diodes: A Lagrangian revision with corrections," *Phys. Plasmas*, vol. 8, no. 8, pp. 3788–3798, Aug. 2001.
[40] T. Lafleur, "Space-charge limited current with a finite injection velocity revisited," *Plasma Sources Sci. Technol.*, vol. 29, no. 6, Jun. 2020, Art. no. 065002.
[41] J. B. Huang, R. H. Yao, P. Zhao, and Y. B. Zhu, "Simulation of space-charge-limited current for hot electrons with initial velocity in a vacuum diode," *IEEE Trans. Electron Devices*, vol. 68, no. 7, pp. 3604–3610, Jul. 2021.
[42] Y. B. Zhu, M. Y. Liao, P. Zhao, and R. H. Yao, "Nonuniform space charge limited current for 2-D bipolar flow in vacuum diode," *IEEE Trans. Electron Devices*, vol. 68, no. 12, pp. 6538–6545, Dec. 2021.
[43] A. L. Garner, G. Meng, Y. Fu, A. M. Loveless, R. S. Brayfield, and A. M. Darr, "Transitions between electron emission and gas breakdown mechanisms across length and pressure scales," *J. Appl. Phys.*, vol. 128, no. 21, Dec. 2020, Art. no. 210903.
[44] A. M. Darr, C. R. Darr, and A. L. Garner, "Theoretical assessment of transitions across thermionic, field, and space-charge-limited emission," *Phys. Rev. Res.*, vol. 2, no. 3, Jul. 2020, Art. no. 033137.
[45] S. A. Lang, A. M. Darr, and A. L. Garner, "Incorporating photoemission into the theoretical unification of electron emission and space-charge limited current," *J. Vac. Sci. Technol. B, Microelectron.*, vol. 39, no. 6, Dec. 2021, Art. no. 062808.
[46] A. M. Loveless, A. M. Darr, and A. L. Garner, "Theoretical linkage of thermionic, field, and space-charge limited emission for a vacuum crossed-field gap," *IEEE Trans. Plasma Sci.*, early access, Apr. 21, 2022, doi: 10.1109/TPS.2022.3165593.

ADAM M. DARR (Graduate Student Member, IEEE) received the B.S. degree in nuclear engineering from Purdue University, West Lafayette, IN, USA. He is currently pursuing the Ph.D. degree in nuclear engineering with the Bio-Electrics and ElectroPhysics Laboratory in the School of Nuclear Engineering. His research interests include micro- and nanoscale field, thermal, photo- and space-charge limited emission, and electroporation. He received the 2022 Purdue College of Engineering (COE) Outstanding Graduate Research Award for the School of Nuclear Engineering.

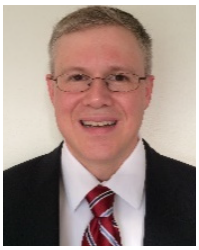

ALLEN L. GARNER (Senior Member, IEEE) received the B.S. degree (Hons.) in nuclear engineering from the University of Illinois at Urbana–Champaign, in 1996, the M.S.E. degree in nuclear engineering from the University of Michigan, Ann Arbor, in 1997, the M.S. degree in electrical engineering from Old Dominion University, Norfolk, VA, USA, in 2003, and the Ph.D. degree in nuclear engineering from the University of Michigan, in 2006.

From December 1997 to December 2003, he worked as an Active Duty Naval Officer serving onboard the USS Pasadena (SSN 752) and as an Instructor with the Prospective Nuclear Engineering Officer Course, Submarine Training Facility, Norfolk. From 2006 to 2012, he was an Electromagnetic Physicist with the GE Global Research Center, Niskayuna, NY, USA. In August 2012, he joined the School of Nuclear Engineering, Purdue University, West Lafayette, IN, USA, where he is currently an Associate Professor and the Undergraduate Program Chair. He is also a Captain with the Navy Reserves and the Commanding Officer of NR SurgeMain Central South, Houston, TX, USA. His research interests include electron emission, gas breakdown, high-power microwaves, and biomedical applications of pulsed power and plasmas.

Prof. Garner is a member of the IEEE International Power Modulator and High Voltage Conference (IPMHVC) Executive Committee and the Dielectrics and Electrical Insulation Society Administrative Committee. He received the 2016 IEEE Nuclear and Plasma Sciences Early Achievement Award, two Meritorious Service Medals, the Navy and Marine Corps Commendation Medal, and Five Navy and Marine Corps Achievement Medals. He served as the Technical Program Chair for the 2016 IEEE IPMHVC, the Treasurer for the 2018 IEEE IPMHVC, and the Technical Program Chair for the 2022 IEEE IPMHVC. He is a Licensed Professional Engineer, Michigan.